An improved upper limit on the direct 3 α decay of the Hoyle state

Bishop, Jack; Smith, Robin; Kokalova, Tzany; Wheldon, Carl; Curtis, Neil; Freer, Martin; Parker, David

DOI:
10.1063/1.5078854

An improved upper limit on the direct 3α decay of the Hoyle state

Jack Bishop, Robin Smith, Tzany Kokalova, Carl Wheldon, Neil Curtis, Martin Freer, and David Parker

Citation: AIP Conference Proceedings **2038**, 020035 (2018); doi: 10.1063/1.5078854
View online: https://doi.org/10.1063/1.5078854
View Table of Contents: http://aip.scitation.org/toc/apc/2038/1
Published by the American Institute of Physics

An improved upper limit on the direct 3α decay of the Hoyle state

Jack Bishop[1,a)], Robin Smith[1,b)], Tzany Kokalova[1], Carl Wheldon[1], Neil Curtis[1], Martin Freer[1] and David Parker[1]

[1]*University of Birmingham, Edgbaston, Birmingham, United Kingdom B15 2TT*

[a)]Corresponding author: jackedwardbishop@gmail.com
[b)]robin.smith@shu.ac.uk

Abstract. The structure of the Hoyle state, a near-threshold 0^+ state of extreme astrophysical significance in ^{12}C has long been investigated. An experiment was performed to measure the branching ratio for the decay of this state directly into 3 α-particles. Such a branching ratio is expected to be a good observable for whether the resonance can be described as a dilute gas of α-particles known as an α-condensate. This experiment gave the best upper limits to date for this direct decay via the improvement of the traditionally used DDΦ model to isotropic decay to the available phase space. The new DDP^2 model includes three-body penetrabilities and gives a limit of $< 0.026\%$ (95% C.L.), a factor of 5 improvement over the previous experimentally obtained limit.

IMPORTANCE OF CLUSTERING

The area of clustering presents a great probe of the nuclear force. An understanding of the nuances of the nuclear force beyond the mean-field approximation can be extracted by studying the structure of light-nuclei. The dominant driver of clustering in the light nuclear region is the inert sub-unit of the α-particle. The residual interaction between this tightly-bound boson and the core of a light system is weak, therefore, around the α-decay threshold, this cluster structure is expected to manifest itself, an idea represented by the well-known Ikeda diagram (**FIGURE 1**). As well as those nuclei where clustering occurs around the α-decay threshold, there is also the possibility for clustering where the entire nucleus dissociates into a system of α-particles, known as an N-α state. The consequences of such structures have huge astrophysical importance in nucleosynthesis.

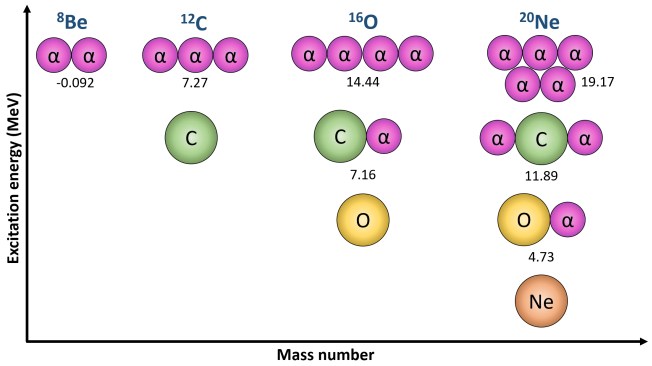

FIGURE 1. Ikeda-diagram showing the expected energies at which different forms of clustering are expected to occur in light-nuclei. Adapted from [1].

Proceedings of the 4th International Workshop on "State of the Art in Nuclear Cluster Physics" (SOTANCP4)
AIP Conf. Proc. 2038, 020035-1–020035-8; https://doi.org/10.1063/1.5078854
Published by AIP Publishing. 978-0-7354-1764-9/$30.00

Nucleosynthesis and clustering

Following the primordial nucleosynthesis of the Big Bang, stars accrete matter and their temperatures rise to a sufficient temperature to fuse hydrogen to form helium. As this source of energy becomes exhausted, the star can now fuse helium to form heavier elements. Two ^{4}He nuclei can therefore fuse together with a sufficiently small rate as limited both by quantum tunneling through the Coulomb barrier and by their distribution of energies. The compound nucleus formed is ^{8}Be. Like all other mass 8 (and 5) nuclei, ^{8}Be is unstable and in this case decays back to two ^{4}He nuclei in $\sim 10^{-16}$ s. The synthesis of heavier elements has therefore reached a bottleneck through which there is no apparent path. An early understanding of this problem was achieved by modeling the probability of an interaction of a third ^{4}He nucleus with the unstable ^{8}Be in what is known as the "triple-alpha process" [2]. Such a reaction, however, is severely impeded both by the requirement for a third ^{4}He interaction to occur within $\sim 10^{-16}$s as well as the larger Coulomb barrier between the ^{8}Be and ^{4}He. A calculation of the expected reaction rate in stars, and therefore the amount of ^{12}C and heavier elements which will be created following this bottleneck however underestimated the abundance of ^{12}C and heavier elements by roughly seven orders of magnitude [3]. Fred Hoyle provided the insight into the rectification of this discrepancy by postulating the existence of a near-threshold state in ^{12}C which provided a resonance that could enhance the reaction rate for the triple-alpha process [4]. Furthermore, this state would most likely have a 0^+ spin-parity. While such a state at $\sim$ 7.6 MeV had been measured previously (and subsequently not-detected in later experiments) [5], this renewed insight into the triple-alpha process allowed for measurement of a state at 7.65 MeV, only 30 keV from where Fred Hoyle had predicted it to exist [6]. It is for this reason that this 0^+_2 state in ^{12}C carries his name.

Structure and importance of the Hoyle state

In order to sufficiently enhance the triple-alpha reaction rate, the Hoyle state must have a large width to the ^{8}Be + α channel. By virtue of ^{8}Be being unbound (and subsequent work demonstrating ^{8}Be has a dumbbell α-particle structure [7]) the Hoyle state can be thought of as a 3α cluster structure. While the dominant contribution to the triple-alpha reaction rate is related to the ^{8}Be + α width, the other decay channels also have a large contribution to the nucleosynthesis rate. The first of these is the radiative width. Following the population of the Hoyle state via the mutual coalescing of 3 α-particles, to produce ^{12}C, the state must radiatively decay. This can be achieved either through sequential gamma-decay through the 2^+_1 or through internal pair conversion directly to the 0^+_1(g.s). Finally, the Hoyle state can also decay directly into 3 α-particles in a three-body decay. While this decay mode is largely suppressed relative to the sequential decay through the ^{8}Be(g.s), the decay width becomes important at higher temperatures [8]. This whole process is portrayed in **FIGURE 2**.

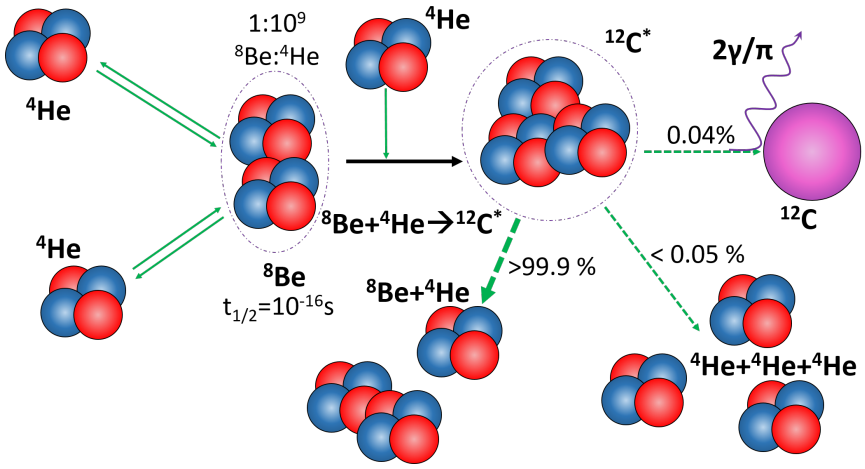

FIGURE 2. Schematic of the stages of the triple-alpha process. A two-step process of the formation of ^{8}Be followed by the formation of ^{12}C* then requires de-excitation to the ground-state for the synthesis of ^{12}C(g.s).

Additionally, there have been many models attempting to explain the structure of the Hoyle state. Early models suggested a linear-chain arrangement of α-particles which has since been excluded as such a configuration is unstable

and with such a large moment of inertia, rotational excitations of the Hoyle state have not been found where such a structure would require them [9]. Later models following a geometrical basis suggested a "bent-arm configuration" where the ^{8}Be stays more tightly bound within the nucleus [10]. The Algebraic Cluster Model (ACM) was used to predict the vibration-rotation spectrum of an equilateral triangle configuration of 3 α-particles which has remarkable success in ascribing different excitation modes to different rotational bands within ^{12}C [11]. A particularly captivating model takes the role of the α-particles in the system further by treating the nucleus as a dilute gas of α-particles which have condensed into the $(0s)^4$ lowest energy level as allowed by their bosonic nature [12]. This transition from a fermionic liquid to a bosonic gas is known as α-condensation and has been predicted to occur in light nuclei up until around ^{40}Ca [13]. This represents a new state of matter inside the nucleus where the density has dropped from ρ_0 to $\sim \frac{\rho_0}{3} \rightarrow \frac{\rho_0}{5}$ allowing for a unique investigation into the nuclear equation of state [14, 15, 16, 17].

To understand the underlying structure of the Hoyle state, one can rely on a precise measurement of the direct 3α decay branching ratio observable. If the Hoyle state is indeed a dilute gas of α-particles, the expected direct 3α decay branching ratio will be larger than a "bent-arm" or equilateral triangle arrangement [18]. The previously published limit is $< 0.2\%$ (95% C.L.) [19] however such a value is insufficient to be able to differentiate between the predicted structures. A new experiment was therefore performed which has a higher level of sensitivity to elucidate the degree to which the Hoyle state can be described as an α-condensate [20] [21].

EXPERIMENT

Experimental set-up

The experiment was designed in such a way as to minimize any source of background identified as contributing to the direct 3α branching ratio. To populate the Hoyle state, the ^{12}C(^{4}He,^{4} He)^{12}C* inelastic scattering reaction was used by virtue of a 40 MeV ^{4}He beam provided by the Birmingham MC40 cyclotron incident on a natural carbon target. The scattered beam was identified using a 65-500 μm dE-E silicon DSSD telescope. The break-up of the Hoyle state was detected on the opposite side of the beam using a quad array of 500 μm DSSDs. This quad array was placed such that population of the Hoyle state placed the scattered beam and the break-up α-particles in kinematic coincidence to maximize the count rate. A thin carbon target (100 μg/cm^2) was used and placed at 45° to the beam direction to minimize the energy loss and energy straggling, another source of background. The experimental set-up is summarized in **FIGURE 3**. In total, 60 hours of beam-time data were taken with an average beam current of 6 enA.

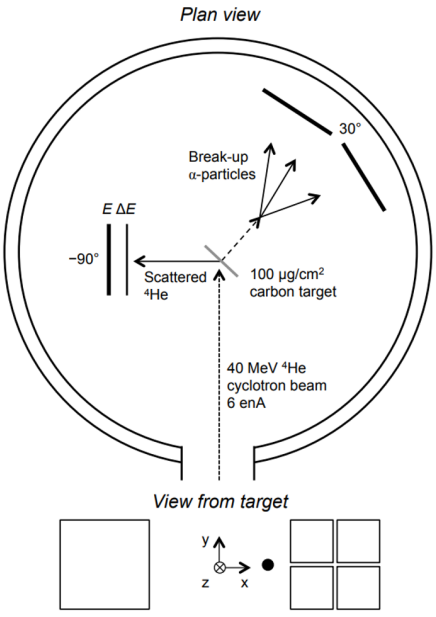

FIGURE 3. Experimental set-up for the ^{12}C(^{4}He,^{4} He)^{12}C* reaction. Figure taken from [21].

Data analysis

To ensure the best resolution and lowest background level, only events with full-kinematics (i.e. detection of all 4 particles) were taken. To ensure these 4 particles arose from the desired ^{12}C(^{4}He,^{4} He)^{12}C* reaction, particle identification was first performed on the scattered beam by placing a cut on the ^{4}He locus seen in **FIGURE 4** from the plot of energy in the dE and E DSSD. Following this selection, requiring 3 hits in the quad array of DSSDs then left 14% of events showing the relatively large efficiency for detection of 3 particles. Following this restrictions, the data were then separated into two different sets. These two data sets constituted a higher count, higher background and a lower count, lower background set. When multiple α-particles hit a detector, there becomes an ambiguity about the hit positions. The lower background subset of data therefore consists of events where each α-particle hits a separate detector and no such ambiguity exists. As this requires a more stringent cut on the phase-space of the system, only 21% of events with 3 hits in the quad belong to this data set (type I). The higher background data set therefore correspond to where 2 α-particles hit a single detector and the 3$^{\text{rd}}$ is measured in a separate detector. This less restrictive subset contributes 73% of the events with 3 particles in the quad hence provide better statistics (type II). The remaining 6% of events occur where all particle hit a single detector and provide a situation whereby the ambiguity about hit positions is greatly enhanced and such these data are ignored.

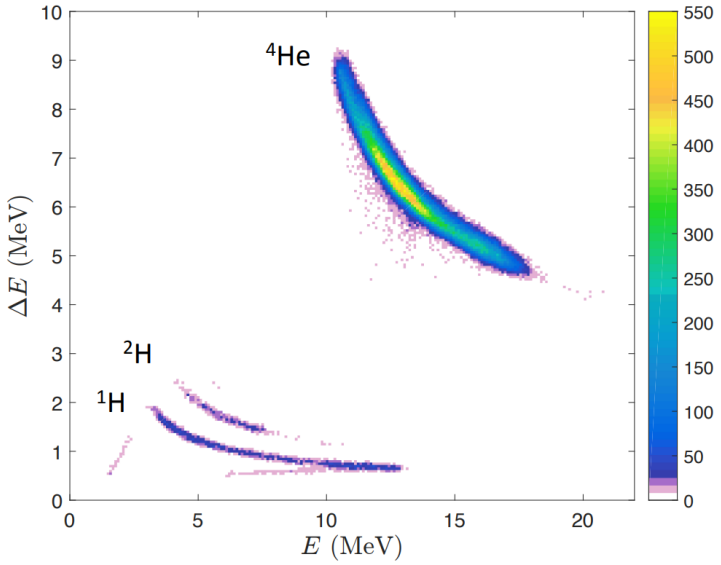

FIGURE 4. 2D histogram of $E - dE$ energy from the silicon DSSD showing the loci populated by different nuclei (labeled).

To ensure the populated state is that of interest, the excitation energy was obtained using two methods. The first method used the scattered beam to obtain the excitation energy and kinetic energy of the scattered ^{12}C* (E_x and E_C respectively) using conservation of energy and momentum from the scattered beam $P_{b'}$;

$$\begin{aligned} \vec{P_C} &= \vec{P}_{\text{beam}} - \vec{P_{b'}}, \\ E_C &= \frac{\vec{P_C}.\vec{P_C}}{2m_C} \quad \text{and} \\ E_x &= E_{\text{beam}} - E_C - E_{b'}. \end{aligned} \tag{1}$$

The second method obtained the excitation energy via the break-up of ^{12}C* (with energy and momentum E_C and $\vec{P_C}$) into 3 α-particles and their corresponding momenta $\vec{P_{\alpha_1}}$, $\vec{P_{\alpha_2}}$ and $\vec{P_{\alpha_3}}$.

$$\vec{P_C} = \sum_{i=1}^{3} \vec{P_{\alpha_i}},$$

$$E_C = \frac{\vec{P_C}.\vec{P_C}}{2m_C} \quad \text{and}$$
$$E_x = E_{\alpha_1} + E_{\alpha_2} + E_{\alpha_3} - E_C. \tag{2}$$

Gates were placed on both these excitation energies to mutually assure the 7.65 MeV Hoyle state was populated. Additionally, a cut was placed on the total reaction Q-value to further clean the data. Finally, a cut was placed on the total x, y and z momenta which was found to be a parameter that was very sensitive to the inclusion of background events. Given the data were now at a maximally clean level, the break-up mechanisms of the selected events in the two data sets were then analyzed.

Dalitz plots

To differentiate the sequential decay mechanism from the direct break-up mechanism, the Dalitz technique was used [22]. This relies on plotting the normalized center-of-mass energies of the 3 break-up α-particles in a "tri-dimensional plot" which has been projected into 2D. This is shown in **FIGURE 5**. The co-ordinates, given by x and y, are obtained from the center-of-mass energies $E_{i_{cm}}$ by:

$$\epsilon_i = \frac{E_{i_{cm}}}{\sum_j E_{j_{cm}}},$$
$$x = \frac{1}{\sqrt{3}}(\epsilon_2 - \epsilon_1) \quad \text{and}$$
$$y = \frac{1}{3}(\epsilon_2 + \epsilon_1 - 2\epsilon_3). \tag{3}$$

Sequential decay events via the ^{8}Be(g.s) share their energy such that the initial decay α-particle takes around 50% of the total energy with the remaining α-particles sharing the remaining 50%. On the Dalitz plot, this corresponds to populating the red loci in **FIGURE 5**. In a direct 3 α-particle decay, there is no such restriction on the energy sharing and any point within the circle constrained by the triangle can be populated. To understand the distribution of the population from this direct decay, three different decay models were used.

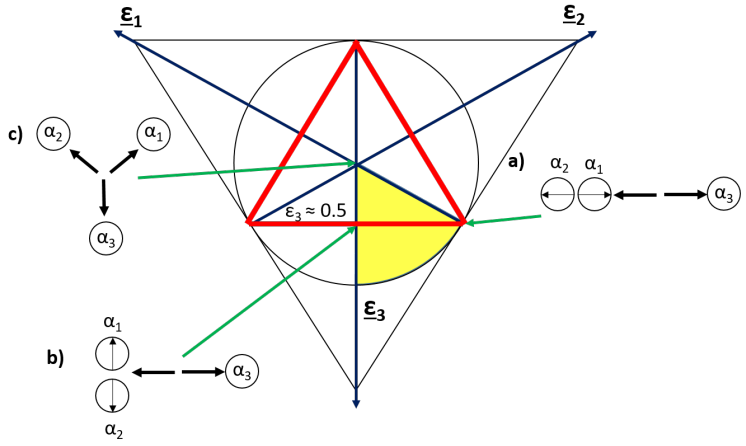

FIGURE 5. Dalitz plot demonstrating the energy sharing in a three-body decay in three scenarios. In a) the Hoyle state is decaying sequentially in a collinear fashion where α_1 is left with a very small fraction of the total energy. b) also corresponds to sequential decay however here the two α-particles from the second decay stage share the energy equally by decaying orthogonally to the original decay direction. Scenario c) corresponds to a direct decay where the α-particles share their energy equally (DDE). The shaded yellow area corresponds to the sector into which all events can be "folded" using the symmetries afforded by the Dalitz plot by ensuring $\epsilon_3 > \epsilon_2 > \epsilon_1$.

Decay models

The first decay mechanism models the direct 3 α-particle break-up by a constant population across the phase space which has a constant density across the Dalitz plot. This model is denoted by DDΦ. The second model assumes the three α-particles decay where they have the same energy which is only smeared by the position-momentum uncertainty principle with the size of the Hoyle system. This model is denoted by DDE. The final model models a collinear decay of the 3 α-particles. During this decay mode, one α-particle is left with a small amount of energy with the other α-particles sharing the remaining energy equally. This model is denoted by DDL. To understand the contribution of each of these three decay modes to the experimental data, a Monte Carlo simulation was performed using the RESOLUTION8.1 package which incorporated the aspect of the decay modes as well as detector efficiency effects [23] [24]. For the two different data sets (type I and type II), the efficiency across different parts of the Dalitz plot is different. Therefore, the expected signal is marginally different for the same decay mode between these two data sets.

As discussed elsewhere [25], the DDΦ model is extremely simplistic. In particular, it excludes all aspects of three-body penetrabilities which one would expect to vary drastically across different regions of the Dalitz plot as the relative energies between the particles can vary by a large amount. To incorporate this effect, an improvement to the model was introduced by including this penetrability effect to produce the DDP^2 model.

To calculate this three-body penetrability, the system was converted to hyperspherical co-ordinates [26]. In this formulation, the hyper-radius ρ increases linearly in time for all initial condition orientations. The tunneling probability through a Coulomb barrier for a three-body system can therefore be formulated dependent only on scaling constants s_{ij} which describe the relative distance between particles i and j. Different positions in the Dalitz plot correspond to different values for these scaling constants and therefore the penetrability can be calculated over the surface of the Dalitz plot. The DDP^2 is then the product of this penetrability and the DDΦ model which can be seen in **FIGURE 6**.

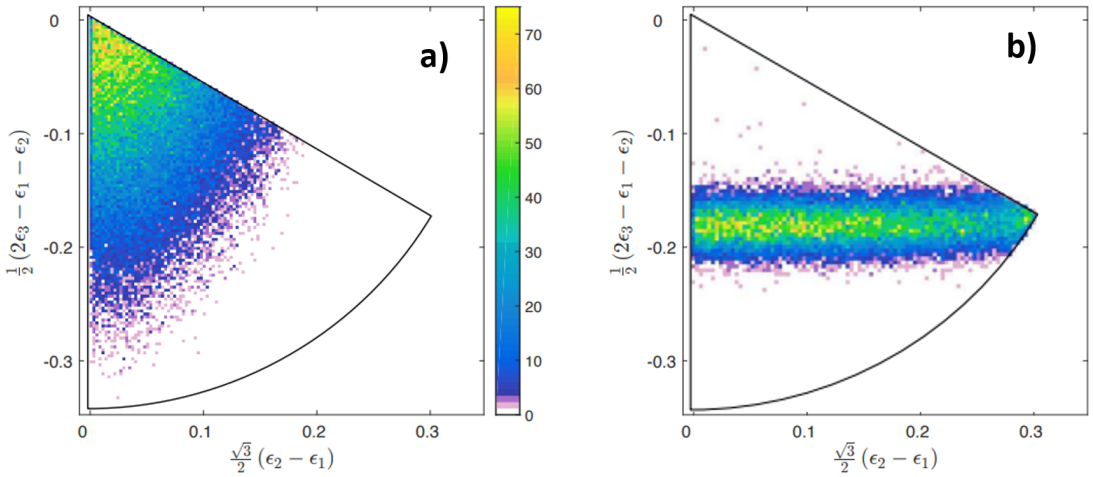

FIGURE 6. a) Dalitz plot demonstrating the energy sharing in a three-body decay in the DDP^2 model showing the dominance of the center of the Dalitz plot corresponding to equal energy sharing. b) Dalitz experimental data for the data of type I showing the sequential nature of the Hoyle decays with a small number of events which do not lie on the sequential loci.

Branching ratios

Given an understanding of how the different direct decay mechanisms contribute to the Dalitz plots, the experimental data were then compared to a Monte Carlo simulation for sequential decay only. This Monte Carlo simulation also included event-mixing at a level consistent with fitting the excitation functions. For the subset of type I corresponding to three hits in separate DSSDs, there were a total of 24,000 Hoyle decay events. For the subset of type II with two hits in a single DSSD, there were 69,000 Hoyle decay events. The Dalitz plot was projected onto the y-axis to

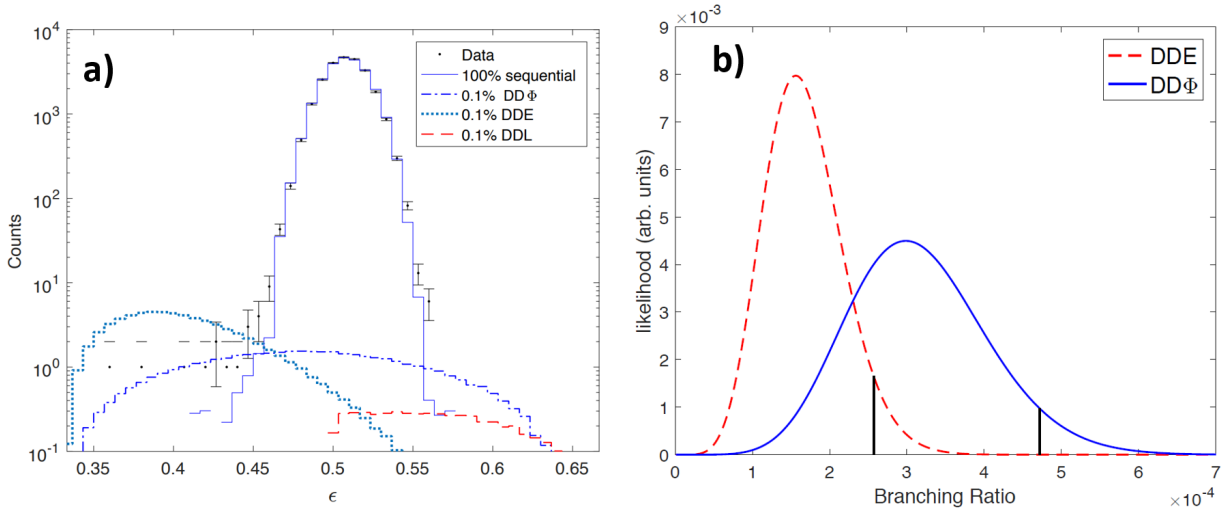

FIGURE 7. a) Projection of the Dalitz plot onto the y-axis for the subset type I (black points). The requirement for a direct component above that predicted from the Monte Carlo sequential decay with event-mixing (solid blue) can clearly be seen. b) Log-likelihood for different branching ratios for the two direct decays, DDE and DDΦ. The black lines denote the 95% confidence limit.

allow for the differentiation between sequential and direct decays. The projection for the DDE and DDP^2 models are almost identical and therefore can be treated as having the same behavior. The comparison of this model can be seen (**FIGURE 6a**) alongside the experimental data (**FIGURE 6b**) where a very small number of events are seen in excess of those predicted solely by sequential decay. To extract a direct decay branching ratio, the different direct decay mechanisms were included at different branching ratios and the change in the log-likelihood was plotted as a function of this added strength. The result from this is shown in **FIGURE 7** where the black lines signify the 95% confidence level (C.L.) for the DDE and DDL. This allows for a rejection of a branching ratio higher than 0.026% for the DDE/DDP^2 and 0.047% for the DDΦ mode at the 95% C.L. (summarized in **TABLE 1**). The previous limit was that given by Itoh of $< 0.2\%$ [19] for the DDΦ model which has been improved by a factor of 4 in the current experiment with a record 93,000 Hoyle decay events. Additionally, the work developing the simplicities of this DDΦ model by incorporating three-body penetrabilities to create the DDP^2 model has demonstrated this direct component can actually be further improved to be $< 0.026\%$ constituting a factor of 8 improvement.

TABLE 1. Direct decay results for the different decay mechanisms

	BR optimal	95 % C.L.	99.5 % C.L.
DDΦ	3.0×10^{-4}	4.7×10^{-4}	5.8×10^{-4}
DDE/DDP^2	1.6×10^{-4}	2.57×10^{-4}	3.2×10^{-4}
DDL	0	3.8×10^{-5}	6.4×10^{-5}

These results can also be compared to those performed at the same time where a DDΦ branching ratio of $< 0.043\%$ (95% C.L.) was achieved using a different population mechanism [27]. These results therefore signify either arriving at the true branching ratio (rather than an upper limit) or more likely reaching the limits afforded by traditional charged particle spectroscopy using silicon detectors. Instead, more sensitive probes may require either greatly enhanced statistics (by virtue of increased solid-angle coverage) or the use of time-projection chambers where the ambiguities of multiple interactions can be removed to a greater degree.

Given the ever decreasing value for the branching ratio of this direct decay component, the interpretation of the Hoyle state as an α-condensate is looking increasingly less likely. Since the original publication of these results however, there has been a renewed level of theoretical input which suggests a condensed Hoyle state will have a direct

decay component of $\sim 0.004\%$ (95% C.L.) for DDE [28] [29] requiring a factor of 7 improvement from the current result.

ACKNOWLEDGMENTS

The assistance of the staff during this experiment at the University of Birmingham MC40 Cyclotron is gratefully acknowledged. This work was funded by the United Kingdom Science and Technology Facilities Council (STFC) under Grant No. ST/L005751/1.

REFERENCES

[1] K. Ikeda, N. Takigawa, and H. Horiuchi, Prog. Theor. Phys. Supp. **E68**, 464–475 (1968).
[2] H. Bondi and E. E. Salpeter, Nature **169**, 304 EP – (1952).
[3] E. E. Salpeter, Annu. Rev. Nucl. Sci. **2**, 41–62 (1953).
[4] F. Hoyle, Astrophys. J. Suppl. S. **1**, p. 121 (1954).
[5] H. Kragh, When is a prediction anthropic? Fred Hoyle and the 7.65 MeV carbon resonance, May 2010.
[6] D. N. F. Dunbar, R. E. Pixley, W. A. Wenzel, and W. Whaling, Phys. Rev. **92**, 649–650 (1953).
[7] R. Guardiola, I. Moliner, and M. Nagarajan, Nuclear Physics A **679**, 393 – 409 (2001).
[8] S. Ishikawa, Phys. Rev. C **87**, p. 055804 (2013).
[9] M. Freer, S. Almaraz-Calderon, A. Aprahamian, N. I. Ashwood, M. Barr, B. Bucher, P. Copp, M. Couder, N. Curtis, X. Fang, F. Jung, S. Lesher, W. Lu, J. D. Malcolm, A. Roberts, W. P. Tan, C. Wheldon, and V. A. Ziman, Phys. Rev. C **83**, p. 034314 (2011).
[10] E. Epelbaum, H. Krebs, D. Lee, and U.-G. Meißner, Phys. Rev. Lett. **106**, p. 192501 (2011).
[11] D. J. Marín-Lámbarri, R. Bijker, M. Freer, M. Gai, Tz. Kokalova, D. J. Parker, and C. Wheldon, Phys. Rev. Lett. **113**, p. 012502 (2014).
[12] A. Tohsaki, H. Horiuchi, P. Schuck, and G. Röpke, Phys. Rev. Lett. **87**, p. 192501 (2001).
[13] T. Yamada and P. Schuck, Phys. Rev. C **69**, p. 024309 (2004).
[14] G. Röpke, A. Schnell, P. Schuck, and P. Nozières, Phys. Rev. Lett. **80**, 3177–3180Apr (1998).
[15] T. Sogo, R. Lazauskas, G. Röpke, and P. Schuck, Phys. Rev. C **79**, p. 051301 (2009).
[16] T. Sogo, G. Röpke, and P. Schuck, Phys. Rev. C **82**, p. 034322 (2010).
[17] P. Schuck, J. Phys. Conf. Ser. **436**, p. 012065 (2013).
[18] Tz. Kokalova, N. Itagaki, W. von Oertzen, and C. Wheldon, Phys. Rev. Lett. **96**, p. 192502 (2006).
[19] M. Itoh, S. Ando, T. Aoki, H. Arikawa, S. Ezure, K. Harada, T. Hayamizu, T. Inoue, T. Ishikawa, K. Kato, H. Kawamura, Y. Sakemi, and A. Uchiyama, Phys. Rev. Lett. **113**, p. 102501 (2014).
[20] R. Smith, Tz. Kokalova, C. Wheldon, J. E. Bishop, M. Freer, N. Curtis, and D. J. Parker, Phys. Rev. Lett. **119**, p. 132502 (2017).
[21] R. Smith, "Experimental measurements of break-up reactions to study alpha clustering in carbon-12 and beryllium-9," December (2017), Birmingham e-thesis repository.
[22] R. H. Dalitz, Phil. Mag. Ser. 7 **44**, 1068–1080 (1953).
[23] N. Curtis *et al.*, Phys. Rev. C **51**, 1554–1557 (1995).
[24] N. Curtis *et al.*, Phys. Rev. C **53**, 1804–1810 (1996).
[25] J. Refsgaard, H. Fynbo, O. Kirsebom, and K. Riisager, Phys. Lett. B **779**, 414 – 419 (2018).
[26] E. Nielsen, D. Fedorov, A. Jensen, and E. Garrido, Phys. Rep. **347**, 373 – 459 (2001).
[27] D. Dell'Aquila *et al.*, Phys. Rev. Lett. **119**, p. 132501 (2017).
[28] S. Ishikawa, Phys. Rev. C **90**, p. 061604 (2014).
[29] H. Zheng, A. Bonasera, M. Huang, and S. Zhang, Physics Letters B **779**, 460 – 463 (2018).